Interval state estimation based on constraint propagation for a lithium-ion cell using an equivalent circuit model ⋆

D. Locatelli * **B. S. Rego** ** **G. V. Raffo** ** **D. M. Raimondo** *

* *Dept. of Electrical, Computer and Biomedical Engineering, University of Pavia, Italy (email: diego.locatelli01@universitadipavia.it)*
** *Graduate Program in Electrical Engineering, Dept. of Electronics Engineering, Federal University of Minas Gerais, Brazil*

Abstract: Battery management systems (BMSs) are responsible for controlling and monitoring battery operations. In order to be effective, BMSs rely on mathematical models. The parameters of these latter are usually obtained through an identification procedure which provides limited accuracy. In addition, only cell current and voltage are usually measurable. For this reason, the model states need to be estimated. In the following, we propose an interval state estimation of a lithium-ion cell when using an equivalent circuit model, taking into account bounded parametric uncertainty and measurement noise. Simulation results show the suitability of the proposed interval estimator to provide a tight enclosure of the states, which is essential for fault detection and model-based control of a lithium-ion cell.

Keywords: Lithium-ion batteries, battery management system, state of charge estimation, interval-based nonlinear state estimation.

1. INTRODUCTION

Li-ion batteries have become of particular interest due to their use in many commercial sectors, including portable electronic devices, hybrid and electric vehicles, and grid energy storage. High cell voltage, cycling durability, high energy and power density are the main key factors that make Lithium-ion the best trade-off between costs, performance and efficiency compared to other battery types on the market.

Battery Management Systems (BMSs) aim to make the battery safe, reliable and efficient. As shown in Lu et al. (2013), violation of temperature, current and voltage restrictions may result in lower performance as well as safety issues. Advanced BMSs rely on mathematical models in order to improve efficiency and monitor the battery cell by estimating fundamental quantities such as the State of Charge (SOC). Mathematical models for Lithium-ion battery dynamics fall within two main categories: Equivalent Circuit Models (ECMs) and Electrochemical Models (EMs). EMs are very accurate and, therefore, very useful when high fidelity is required, such as in simulations. They are generally very complex models, which affects the computational cost. On the other, hand ECMs are simpler and used in real-time control system applications, especially for online SOC and state estimation.

Look-up table methods are used for SOC estimation exploiting its relations with other measurable parameters as the Open Circuit Potential (OCP), but they are not suitable for run-time operations (Xiong et al., 2017). This is due to the fact that the OCP can be measured only in stationary conditions. Coulomb counting is also one of the main tools used for SOC estimation (Piller et al., 2001), but it is not completely accurate because of drift errors due to disturbances on the current measurement and uncertainty on the cell capacity. Moreover, while SOC estimation is important, in order to employ a model-based controller, full state estimation is required.

Several stochastic approaches on state estimation have been applied in the battery field, including Extended Kalman filtering (Di Domenico et al., 2010; Bizeray et al., 2015), sliding-mode observer (Kim, 2009), Sigma-point Kalman filtering (Plett, 2006), Particle filtering (Tulsyan et al., 2016), and Moving Horizon Estimator (Hu et al., 2018).

The stochastic estimation approaches assume that probabilistic distributions of the uncertainties are known. On the other side, set-based estimation considers unknown but bounded uncertainties. When physical bounds are available (as for the case of ECM parameters), this second option is more reliable since knowing the exact distribution of the uncertainties is rarely the case in practice.

Different set representations have been used for state estimation such as intervals (Jaulin et al., 2001), polytopes (Shamma and Tu, 1997), zonotopes (Alamo et al., 2008), and constrained zonotopes (Rego et al., 2020). The choice of set representation depends on the accuracy required for describing the set of interest, as well as the computational burden. Another important factor, especially for highly nonlinear systems, is to choose a methodology that can

⋆ This work has been supported by the Italian Ministry for Research in the framework of the 2017 PRIN, Grant no. 2017YKXYXJ, the brazilian project INCT under the grant CNPq 465755/2014-3, FAPESP 2014/50851-0, and also by the brazilian agencies CAPES under the grants 001 and 88887.136349/2017-00, and FAPEMIG.

better deal with the conservatism. This can be caused, for example, by the dependency effect, the wrapping effect, and linearization errors. To the best of our knowledge, set-based estimation was used within the battery context only in Zhang et al. (2020). This latter proposes a continuous-time ECM-based interval observer for SOC estimation in a parallel connected Li-ion battery pack. The proposed observer assumes that continuous-time measurements are available, which is not true in practice since sensors have finite sampling rates. Moreover, the coupling between parameters is not considered, which is usually present when an identification procedure is performed.

In this paper, we develop a discrete-time interval observer for a single Li-ion cell based on the forward-backward method described in Jaulin et al. (2001). In particular, parametric uncertainties are considered and obtained by performing an identification procedure on data collected on a well known EM, i.e. the Single Particle Model with electrolyte dynamics (SPMe) (Pozzi et al., 2018). The contributions of this paper are: (i) the identification of ECM parameter bounds based on the Fisher Information Matrix; and (ii) a discrete-time interval state estimation method based on inclusion functions and constraint propagation, which handles discrete-time measurement. Numerical experiments show that the proposed methodology is efficient and provides accurate enclosures for both the SOC and the electric state variables of the ECM.

2. LITHIUM-ION CELL MODEL

A Single Particle Model with electrolyte dynamics (SPMe) has been used in this work to simulate the "real plant". Terminal voltage data have been collected on the SPMe in order to identify the parameters of the ECM used for state estimation purposes (as described later in Section 3). This electrochemical model is general for cells utilizing two composite electrodes (cathode and anode) with active insertion material, electrolyte and inert conducting material. SPMe allows to trace the dynamics of chemical quantities, such as surface and average stoichiometries and ions concentrations, in the electrolyte and solid phases. For the complete description of the SPMe we rely on Pozzi et al. (2018) in which the parameters refer to a Kokam SLPB 75106100 cell. Note that in this paper, differently from (Pozzi et al., 2018), we assume that the cell is kept in a climatic chamber at constant temperature (isothermal process).

The ECM considered in this work for state estimation purposes is the Thévenin model depicted in Fig. 1. It consists of three parts: (i) the open circuit potential $V_{\mathrm{oc}}(t)$; (ii) two internal resistors R_0 and R_1; and (iii) the capacitor C_1. This latter is useful to describe the charge and discharge transient of the cell. The electrical behavior of the ECM is derived from Kirchhoff and Ohm's laws, as it is shown in the following system equations:

$$\begin{cases} \dot{z}(t) = -\dfrac{I(t)}{C_{\mathrm{batt}}}, \\ \dot{V}_{c_1}(t) = -\dfrac{V_{c_1}(t)}{R_1(t)C_1(t)} + \dfrac{I(t)}{C_1(t)}, \end{cases} \tag{1}$$

where $z(t)$ is the cell SOC, $V_{c_1}(t)$ the voltage drop across the parallel $R_1 - C_1$, C_{batt} is the nominal cell capacity,

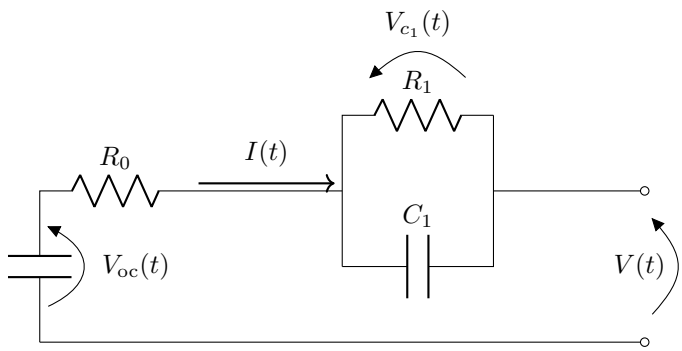

Fig. 1. Thévenin equivalent circuit model of the Lithium-ion cell.

and $I(t)$ is the input current. Note that we adopt the convention that the battery is charged by a negative current.

In accordance with Perez et al. (2017), in order the ECM to better approximate the SPMe, R_1 and C_1 can be expressed as nonlinear functions of the SOC

$$R_1(t) = R_{1,0} + R_{1,1}z(t) + R_{1,2}z(t)^2, \tag{2}$$

$$C_1(t) = C_{1,0} + C_{1,1}z(t) + C_{1,2}z(t)^2. \tag{3}$$

Finally, the output voltage equation can be computed as

$$V(t) = V_{\mathrm{oc}}(t) - R_0\, I(t) - V_{c_1}(t), \tag{4}$$

where the overall open circuit potential, $V_{\mathrm{oc}}(t)$, is expressed here as a ninth degree polynomial function of the SOC, given by:

$$\begin{aligned} V_{\mathrm{oc}}(t) = {} & 3.592 + 0.9082\, z(t) - 0.57\, z(t)^2 + \\ & - 2.979\, z(t)^3 + 6.56\, z(t)^4 - 4.238\, z(t)^5 + \\ & + 0.8608\, z(t)^6 - 1.676{\cdot}10^{-10}\, z(t)^7 + \\ & + 1.143{\cdot}10^{-10}\, z(t)^8 - 2.982{\cdot}10^{-11}\, z(t)^9. \end{aligned} \tag{5}$$

This latter is obtained by a fitting procedure, starting from equation (14) in Pozzi et al. (2018). This is necessary since the surface stoichiometries θ_p and θ_n are not considered in our ECM (1). Note that in stationary conditions (i.e. when no current is applied), surface stoichiometries can be defined as SOC functions. Compared with the OCP nonlinear function of the SPMe, the polynomial function in (5) is still very accurate (Root Mean Square Error RMSE $= 3.896{\cdot}10^{-4}$). Moreover, being a simpler expression, it results in less conservatism when evaluated through interval arithmetic.

The identification of the ECM parameters, besides the V_{oc} which is assumed known a priori as in (5), relies on the procedure described in Section 3.

3. IDENTIFICATION OF THE ECM PARAMETERS

The ECM described in Section 2 can be formally written as

$$\begin{cases} \dot{\mathbf{x}}(t) = \mathbf{f}(\mathbf{x}(t), \mathbf{u}(t), \boldsymbol{\phi}), \\ \mathbf{y}(t) = \mathbf{g}(\mathbf{x}(t), \mathbf{u}(t), \boldsymbol{\phi}), \\ \mathbf{x}(t_0) = \mathbf{x}_0, \end{cases} \tag{6}$$

$$\boldsymbol{\phi} \triangleq [R_0\ R_{1,0}\ R_{1,1}\ R_{1,2}\ C_{1,0}\ C_{1,1}\ C_{1,2}\ C_{\mathrm{batt}}]\,. \tag{7}$$

In order to apply the interval state estimation method proposed in this work the ECM is firstly discretized according to the Euler's method, thus obtaining

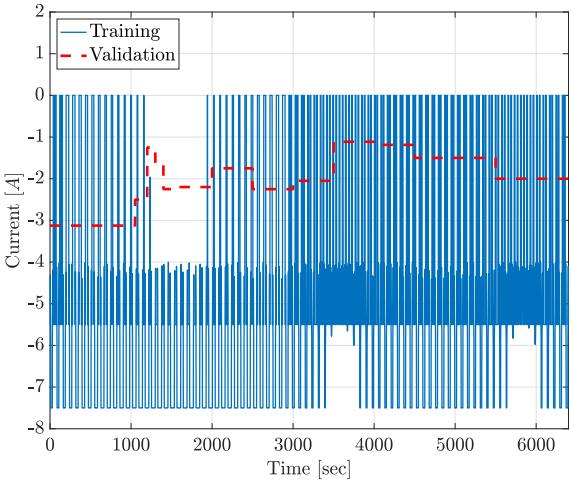

Fig. 2. Training and validation current input profiles.

$$\begin{cases} \mathbf{x}(k+1) = \mathbf{x}_k + T_s \mathbf{f}(\mathbf{x}(k), u(k), \boldsymbol{\phi}), \\ \mathbf{y}(k) = \mathbf{g}(\mathbf{x}(k), u(k), \boldsymbol{\phi}), \\ \mathbf{x}(k_0) = \mathbf{x}_0, \end{cases} \tag{8}$$

where T_s is the sampling time, and $k \geq k_0$ is the time step.

According to Perez et al. (2017), R_1 and C_1 exhibit a different SOC relation for the charging and discharging phase. In this work, we consider the charging phase only. The parameter estimation is performed starting from data collected on the "real plant", here assumed to be the SPMe. We consider as initial condition an almost completely discharged cell at rest, i.e. $\mathbf{x_0} = [0.017\ 0]^{\mathrm{T}}$ (ECM states), and as input signal, defined over a time horizon $\bar{k}$, the one reported in Fig. 2. Note that a sufficiently exciting input profile helps the identifiability and reduces parametric uncertainties.

Remark 1. Even though the ECM parameters still need to be estimated, $\mathbf{x_0}$ can be easily obtained when a cell is at rest. In this case, the voltage across the parallel $R_1 - C_1$ is zero, V coincides with V_{oc}, and $z(0)$ can be computed from equation (5) [1].

The system is affected by measurement noise that ranges within the interval $[-3mV, 3mV]$. In order to use the following identification procedure, in this section, we approximate it as i.i.d. Gaussian noise $\mathbf{d}(k) \sim \mathcal{N}(0, \sigma_y^2)$ with $\sigma_y = 1mV$. In particular, for the true value of the parameter vector $\boldsymbol{\phi}^*$, one has measurements $\hat{\mathbf{y}}(k, \boldsymbol{\phi}^*) = g(\mathbf{x}(k), \mathbf{u}(k), \boldsymbol{\phi}^*) + \mathbf{d}(k)$. Let $\hat{\mathbf{Y}}(\boldsymbol{\phi}^*) \in \mathbb{R}^{\bar{k}+1}$ denote the vector of observed output data over the time horizon $k = k_0, \ldots, k_0 + \bar{k}$. Then, it holds that $\hat{\mathbf{Y}}(\boldsymbol{\phi}^*) \sim \mathcal{N}(\mathbf{Y}(\boldsymbol{\phi}^*), \mathbf{C}_y)$, where $\mathbf{Y}(\boldsymbol{\phi}^*)$ stands for the output vector in the absence of measurement noise and $\mathbf{C}_y \in \mathbb{R}^{(\bar{k}+1)\times(\bar{k}+1)}$ for the diagonal measurement covariance matrix given by $\mathbf{C}_y = \sigma_y^2 \mathbf{I}_{\bar{k}+1}$.

Once the training data is collected, the parameters can be estimated by solving the following maximum likelihood optimisation problem

[1] The OCP is assumed known a priori.

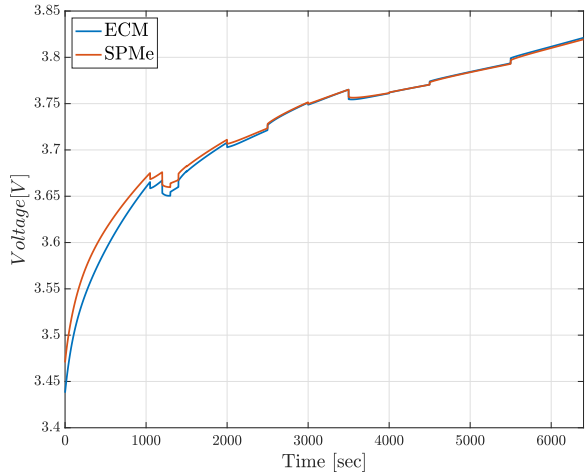

Fig. 3. Validation profile of the terminal voltage.

$$\begin{aligned} \hat{\phi} = \arg\min_{\phi} \ & (\hat{\mathbf{Y}}(\phi^*) - \mathbf{Y}(\boldsymbol{\phi}))^{\mathrm{T}} \mathbf{C}_y^{-1} (\hat{\mathbf{Y}}(\phi^*) - \mathbf{Y}(\boldsymbol{\phi})) \\ \text{s.t.} \ & \text{model dynamics (8)}, \\ & 0 \leq \mathbf{h}(\mathbf{x}(k), \mathbf{u}(k), \boldsymbol{\phi}), \qquad (9a) \\ & \boldsymbol{\phi}^{\min} \leq \boldsymbol{\phi} \leq \boldsymbol{\phi}^{\max}, \qquad (9b) \end{aligned}$$

where $\mathbf{Y}(\boldsymbol{\phi})$ stands for the output vector obtained by solving, for a given ϕ, system (8) over the time horizon $k = k_0, \ldots, k_0 + \bar{k}$. Equation (9b) allows to account for physical bounds on the parameters, e.g. $R_0 \geq 0$, $C_{\mathrm{batt}} \geq 0$. Similarly, equation (9a) is required to bound SOC-dependent variables such as R_1 and C_1. In practice, assuming functions (2) and (3), have the same concavity as in Perez et al. (2017), one can force the positivity of these quantities by setting constraints on their values for $z = 1$ and $z = 0$ (concave case), or for the z corresponding to the minimum value of the function (convex case). This latter can be found analytically. Further constraints can be added when prior knowledge on the parametric bounds is available. The value of the estimated parameters, obtained by solving problem (9), for data collected by applying the experiments in Fig.2 (blue), is reported in Table 1.

Table 1. Estimated ECM parameters.

$R_0(\Omega)$	$R_{1,0}(\Omega)$	$R_{1,1}(\Omega)$	$R_{1,2}(\Omega)$
0.093	0.0221	−0.07	0.0672
$C_{1,0}$(As)	$C_{1,1}$(As)	$C_{1,2}$(As)	C_{batt}(As)
235.52	$7.7613\,10^4$	$-7.0974\,10^4$	$2.6963\,10^4$

The ECM model with the estimated parameters has been tested in validation against the SPMe, using the validation profile in Fig. 2 (red) and the same initial condition of the training phase. As shown in Fig. 3 the results are good but some discrepancy is present. For state-estimation and control purposes, it is important to quantify how accurate the obtained parameter values are. Since $\hat{\mathbf{Y}}(\boldsymbol{\phi}^*)$ is a random variable, one has that also the estimated $\hat{\boldsymbol{\phi}}$ is a random variable with covariance matrix $\mathbf{C}_{\hat{\boldsymbol{\phi}}} \in \mathbb{R}^{8\times 8}$. Similarly to Pozzi et al. (2018), we rely on the Fisher Information Matrix (FIM) to obtain an estimate of $\mathbf{C}_{\hat{\boldsymbol{\phi}}}$. According to the Cramer-Rao bound, the FIM provides a lower bound on the parameters covariance matrix

$$\mathbf{C}_{\hat{\phi}} \geq (\mathbf{F}(\hat{\boldsymbol{\phi}}))^{-1} = ((\mathbf{S}(\hat{\boldsymbol{\phi}}))^{\mathrm{T}} \mathbf{C}_y^{-1} \mathbf{S}(\hat{\boldsymbol{\phi}}))^{-1}, \tag{10}$$

Fig. 4. Parametric correlation matrix.

where $\mathbf{F}(\hat{\boldsymbol{\phi}}) \in \mathbb{R}^{8\times 8}$ is the FIM, and $\mathbf{S}(\hat{\boldsymbol{\phi}})$ is the sensitivity matrix computed as $\mathbf{S}(\hat{\boldsymbol{\phi}}) \triangleq \nabla_{\hat{\boldsymbol{\phi}}}\mathbf{Y}(\hat{\boldsymbol{\phi}})$.

Remark 2. Despite the FIM inverse being commonly used in the literature to quantify the parametric uncertainty, this method can be inaccurate for several reasons: (i) it provides only a lower bound of $\mathbf{C}_{\hat{\boldsymbol{\phi}}}$; (ii) it relies on local parameter sensitivity (which assumes a linear relationship between model parameter variations and simulation results); (iii) it is not able to capture the non-Gaussian case since it estimates only the covariance matrix; (iv) it assumes that the model structure used in the identification phase is correct. Future work will consider better estimates by considering higher-order terms in local sensitivity analysis, by using global sensitivity analysis and take into account the error committed when approximating a high-fidelity model with a reduced one (see e.g. Weber et al. (2019)).

The estimated correlation matrix $\mathbf{R}_{\hat{\boldsymbol{\phi}}}$ [2], obtained using the FIM, is reported in Fig. 4. Non-zero off-diagonal values testify a correlation between the parameters in (7). In order to take into account this feature when using the interval state estimation of the next section, a linear change of variable is made $\hat{\boldsymbol{\psi}} = \mathbf{T}\hat{\boldsymbol{\phi}}$ where $\mathbf{T}$ is chosen as the inverse of the eigenvector matrix of $\mathbf{C}_{\hat{\boldsymbol{\phi}}}$ [3]. By doing so, one obtains that the covariance matrix $\mathbf{C}_{\hat{\boldsymbol{\psi}}}$ of the new parameter set $\hat{\psi}$ is diagonal.

The use of an unbounded distribution to describe the parametric uncertainty is overly conservative since physical electric parameters cannot be negative nor exceed meaningful values (it does not make any sense for the Kokam SLPB 75106100 cell we consider to have a resistance of MΩ). For this reason, in the following section, we restrict each element of the parametric uncertainty $\hat{\boldsymbol{\psi}}_i$ to the following domain $[\hat{\psi}_i - 3\sqrt{C_{\hat{\boldsymbol{\psi}}}(i,i)}, \hat{\psi}_i + 3\sqrt{C_{\hat{\boldsymbol{\psi}}}(i,i)}]$, thus truncating to $\pm$ 3 times the standard deviation of the parameter. These sets are further reduced by considering the physical limits of the original parameters $\hat{\phi}$ (e.g. positivity for each SOC value). Note that, getting a reference system with a diagonal covariance matrix is very important since intervals are not able to capture any coupling between variables.

The identification phase has been implemented using CasAdi (Andersson et al., 2019). The optimisation problem has been solved with IPOPT, a primal-dual interior point method interfaced with CasADi.

4. SET-BASED STATE ESTIMATION METHOD

The set-based state estimation method proposed in this paper relies on intervals. In the following, some basic operations and notations of interval analysis are introduced.

Let $\underline{x}, \overline{x} \in \mathbb{R}$, such that $\underline{x} \leq \overline{x}$. An interval $[x] \subset \mathbb{R}$ is a nonempty set of real numbers defined by $[x] \triangleq \{x \in \mathbb{R} : \underline{x} \leq x \leq \overline{x}\}$. Moreover, the midpoint and the radius of an interval $[x]$ are defined by $\mathrm{mid}([x]) \triangleq (1/2)(\overline{x}+\underline{x})$ and $\mathrm{rad}([x]) \triangleq (1/2)(\overline{x}-\underline{x})$, respectively. The set of all intervals over $\mathbb{R}$ is denoted by $\mathbb{IR}$. The set of all interval vectors in $\mathbb{R}^n$ is denoted by $\mathbb{IR}^n$. A box $[X] \in \mathbb{IR}^n$ is defined as $[X] = ([\underline{x}_1, \overline{x}_1], \ldots, [\underline{x}_n, \overline{x}_n])$. The midpoint and radius of $[X]$ are defined by $\mathrm{mid}([X]) \triangleq (\mathrm{mid}([\underline{x}_1, \overline{x}_1]), \ldots, \mathrm{mid}([\underline{x}_n, \overline{x}_n])$ and $\mathrm{rad}([X]) \triangleq (\mathrm{rad}([\underline{x}_1, \overline{x}_1]), \ldots, \mathrm{rad}([\underline{x}_n, \overline{x}_n])$, respectively. A real arithmetic operation $\odot$ is extended to intervals $[x_1], [x_2] \in \mathbb{IR}$ by $[x_1]\odot[x_2] \triangleq \{x_1 \odot x_2 : x_1 \in [x_1], x_2 \in [x_2]\}$. The intersection of two intervals is defined as $[x_1] \cap [x_2] \triangleq [\max\{\underline{x}_1, \underline{x}_2\}, \min\{\overline{x}_1, \overline{x}_2\}]$. Inclusion functions and basic operations are defined in Moore et al. (2009).

4.1 Problem formulation

Consider the discrete-time nonlinear model written below

$$\begin{cases} \mathbf{x}(k) = \mathbf{f}(\mathbf{x}(k-1), \mathbf{u}(k-1), \mathbf{w}(k-1)), \\ \mathbf{y}(k) = \mathbf{g}(\mathbf{x}(k), \mathbf{u}(k), \mathbf{v}(k)), \end{cases} \tag{11}$$

for $k \geq 1$, with $\mathbf{y}(0) = \mathbf{g}(\mathbf{x}(0), \mathbf{u}(0), \mathbf{v}(0))$, $\mathbf{f} : \mathbb{R}^n \times \mathbb{R}^{n_u} \times \mathbb{R}^{n_w} \to \mathbb{R}^n$, $\mathbf{g} : \mathbb{R}^n \times \mathbb{R}^{n_u} \times \mathbb{R}^{n_v} \to \mathbb{R}^{n_y}$, where $\mathbf{w} \in [W]$ and $\mathbf{v} \in [V]$ are the unknown-but-bounded process and measurement disturbances, respectively.

The objective is to obtain accurate interval enclosures $[\hat{X}](k)$ of the state variables $\mathbf{x}(k)$ which are consistent with the nonlinear system (11) and the measurement $\mathbf{y}_k$. Given an initial set $[\bar{X}](0)$ such that $\mathbf{x}(0) \in [\bar{X}](0)$, in this paper we proceed through the prediction-update algorithm (Rego et al., 2020), which is based on computing intervals $[\bar{X}](k)$ and $[\hat{X}](k)$ such that

$$[\bar{X}](k) \supseteq \{\mathbf{f}(\mathbf{x}(k-1), \mathbf{u}(k-1), \mathbf{w}(k-1)) : \mathbf{x}(k-1) \in [\bar{X}](k-1),\ \mathbf{w}(k-1) \in [W]\}, \tag{12}$$

$$[\hat{X}](k) \supseteq \{\mathbf{x}(k) \in \bar{X}(k) : \mathbf{g}(\mathbf{x}(\mathbf{k}), \mathbf{u}(k), \mathbf{v}(k)) = \mathbf{y}(k),\ \mathbf{v}(k) \in [V]\}, \tag{13}$$

where (12) is referred to as the *prediction step*, and (13) as the *update step*. We assume that an interval enclosure $[\bar{X}](0)$ of the initial state $\mathbf{x}(0)$ and the current measurement $\mathbf{y}(k)$ for $k \geq 0$ are known.

In this paper, the guaranteed state estimation is performed in an efficient way by combining inclusion functions with

[2] Given $D = \sqrt{\mathrm{diag}(\mathbf{C}_{\hat{\phi}})}$, the correlation matrix can been derived by $\mathbf{R}_{\hat{\phi}} = D^{-1}\mathbf{C}_{\hat{\phi}}D^{-1}$.

[3] Since $\mathbf{C}_{\hat{\boldsymbol{\phi}}}$ is symmetric, then it has a complete set of orthogonal eigenvectors and therefore T is invertible.

forward-backward constraint propagation (FBCP) (Jaulin et al., 2001). For each time k, given the previous state set $[\hat{X}](k-1)$, the prediction step (12) is performed using inclusion functions (Moore et al., 2009), resulting in the predicted interval $[\bar{X}](k)$ such that $\mathbf{x}(k) \in [\bar{X}](k)$. On the other hand, the update step (13) is computed by solving a Constraint Satisfaction Problem (CSP).

To obtain $[\hat{X}](k)$, the general problem is to refine $[\bar{X}](k)$ and $[Y](k)$ by removing values in the respective domains that are not consistent with each other. This corresponds to a CSP $\mathcal{H}$, which is formulated as

$$\begin{aligned}\mathcal{H} : \mathbf{y}(k) =& \mathbf{g}(\mathbf{x}(k), \mathbf{u}(k), \mathbf{v}(k)),\ \mathbf{x}(k) \in [\bar{X}(k)],\\ & \mathbf{y}(k) \in [Y(k)],\ \mathbf{v}(k) \in [V],\end{aligned}$$

whose solution set is defined as $\mathcal{S} \triangleq \{\mathbf{y}(k) \in [Y](k), \mathbf{x}(k) \in [\bar{X}](k) : \mathbf{y} = \mathbf{g}(\mathbf{x}(k), \mathbf{u}(k), \mathbf{v}(k)), \mathbf{v}(k) \in V\}$.

To solve $\mathcal{H}$, during the forward constraint propagation phase, the state set $[\bar{X}](k)$ is first propagated through $\mathbf{g}$ using inclusion functions, considering intermediate variables, yielding an output interval $[Y](k)$ which is refined by intersecting it with the measurement $\mathbf{y}(k)$. During the backward propagation, the nonlinear mapping $\mathbf{g}$ is swept backwards and the interval $[Y](k)$ obtained in forward propagation phase is used to refine $[\bar{X}](k)$. The proposed FBCP algorithm for the ECM is detailed in the next section.

4.2 State estimation of the Lithium-ion cell using FBCP

The FBCP algorithm proposed in Jaulin et al. (2001) is composed of three intermediate steps (*contractor decomposition*, *forward update*, and *backward update*), here applied to the ECM example.

We consider (8) describing the ECM with output function $\mathbf{g}$ given by (4). The process disturbance $\mathbf{w}(k) = \mathbf{T}\hat{\boldsymbol{\phi}}$ is determined by the parametric uncertainties in the ECM by means of the transformation matrix in Section 3, bounded by $\mathbf{w}(k) \in [W] \triangleq \mathbf{T}[\hat{\boldsymbol{\phi}}]$.

On the other hand, the output disturbance $\mathbf{v}_k$ comprises both parametric uncertainties and the output additive measurement noise $\mathbf{d}(k) \in [\mathbf{d}] \subset \mathbb{R}$, with $[\mathbf{d}]$ defined in Section 3, as $\mathbf{v}(k) \triangleq [\mathbf{w}(k)^T\ \mathbf{d}(k)]^T$. Note that, since R_0 is correlated to the other parameters appearing in (7) (see Fig.4), $\mathbf{v}(k)$ depends also on $\mathbf{w}(k)$.

In order to mitigate the dependency effect that arises when considering the polynomial function (5), $V_{\text{oc}}(k)$ is rewritten using the centered form suggested in Hansen and Walster (2003), as

$$V_{\text{oc}}([x_1](k)) = p_0(k) + \sum_{i=1}^{9} p_i(k)([x_1](k) - c)^i, \qquad (14)$$

where $c \triangleq \text{mid}([x_1](k))$, with $[x_1](k) \triangleq [z](k)$ being the first component of $[\bar{X}](k)$, p_i being auxiliary variables given by $p_0(k) \triangleq V_{\text{oc}}(c)$ and $p_i(k) \triangleq (1/i!)V_{\text{oc}}^{[i]}(c)$, $i \in \{1, \ldots, 9\}$, and $V_{\text{oc}}^{[i]}(c)$ denoting the i-th derivative of (5) with respect to $z(k)$, evaluated at c.

1) Contractor decomposition. The function $\mathbf{g}$ derived from (4) is first decomposed into a "primitive" form comprised of simplified expressions in which only one function or one elementary operation is present. This is achieved by introducing intermediate variables $[h_i]$ given by

$$[h_i](k) \triangleq ([x_1](k) - c)^i, \quad i \in \{1, \ldots, 9\}, \qquad (15)$$

which allow to rewrite the polynomial function (5) as

$$[V_{\text{oc}}](k) = p_0(k) + \sum_{i=1}^{9} p_i(k)\,[h_i](k). \qquad (16)$$

2) Forward update. Given the measurement $\mathbf{y}(k)$, we first subtract the noise interval $[\mathbf{d}]$, obtaining $[Y](k) \triangleq \mathbf{y}(k) - [\mathbf{d}]$. Then, we compute the intersection

$$[Y](k) \leftarrow [Y](k) \cap [[V_{\text{oc}}](k) + [x_2](k) + R_0 u(k)], \qquad (17)$$

in order to refine $[Y](k)$. Note that if no measurement is available at time k, this set is initialized as $(-\infty, +\infty)$.

3) Backward update. The decomposed function $\mathbf{g}$ is swept backwards. Every variable appearing on the right-hand-side of $\mathbf{g}$ is made an explicit function of the other variables appearing in the forward update, as follows

$$[V_{\text{oc}}](k) \leftarrow [V_{\text{oc}}](k) \cap [[Y](k) - [x_2](k) - R_0 u(k)], \quad (18a)$$
$$[x_2](k) \leftarrow [x_2](k) \cap [[Y](k) - [V_{\text{oc}}](k) - R_0 u(k)]. \quad (18b)$$

For assessing the state of charge $[x_1](k)$, equation (16) is swept backwards and decomposed into multiple expressions, passing first through the intermediate variables $[h_i](k)$, for $i = 1, \ldots, 9$, as

$$\begin{aligned}[h_i](k) \leftarrow [h_i](k) \cap \Big[\frac{1}{p_i(k)}\Big([V_{\text{oc}}](k) - p_0(k)\\ - \sum_{j \neq i} p_j(k)[h_j](k)\Big)\Big].\end{aligned} \qquad (19)$$

The interval $[h_1](k)$ is further refined as follows. Since $[h_1](k)$ is zero centered by definition (see (15)), the following logic is necessary for retrieving both positive and negative even roots to $[h_1](k)$:

$$\begin{aligned}[h_1](k) \leftarrow& [h_1](k) \cap_{i \in \{2,4,6,8\}} ([h_i](k)^{\frac{1}{i}})\\ =& [h_1](k) \cap_{i \in \{2,4,6,8\}} ([-|\overline{h}_i|^{\frac{1}{i}}, |\overline{h}_i|^{\frac{1}{i}}]).\end{aligned}$$

For odd roots, $[h_1](k) \leftarrow [h_1](k) \cap_{i \in \{3,5,7,9\}} ([\underline{\alpha}_i, \overline{\alpha}_i])$, where (i) $\underline{\alpha}_i \triangleq \underline{h}_i^{\frac{1}{i}}$ if $[h_i](k) > 0$, $\underline{\alpha}_i \triangleq -(|\underline{h}_i|^{\frac{1}{i}})$ otherwise, and (ii) $\overline{\alpha}_i \triangleq -(|\overline{h}_i|^{\frac{1}{i}})$ if $[h_i](k) < 0$, $\overline{\alpha}_i \triangleq \overline{h}_i^{\frac{1}{i}}$ otherwise, with $\underline{h}_i$ and $\overline{h}_i$ being the lower and upper bounds of $[h_i](k)$, respectively. Finally, the refinement of the SOC interval is done through the intersection $[x_1](k) \leftarrow [x_1](k) \cap [h_1](k) + c$. The interval enclosure $[\hat{X}](k)$ for the update step (13) is then given by $[\hat{X}](k) \leftarrow [x_1](k) \times [x_2](k)$.

Remark 3. Steps 2 and 3 can be repeated iteratively to obtain a more refined enclosure $[\hat{X}](k)$ (Jaulin et al., 2001). Nevertheless, for the ECM, one iteration demonstrated to provide sufficiently accurate enclosures, as illustrated in Section 5.

Remark 4. Since intervals cannot capture the fact that $\mathbf{w}(k)$ is constant, as well as the dependencies between $\mathbf{v}(k)$ and $\mathbf{w}(k)$, the application of the FBCP algorithm to the ECM is then conservative. Future work will explore other set representations such as zonotopes, which allow to effectively manage this dependency and to reduce conservatism.

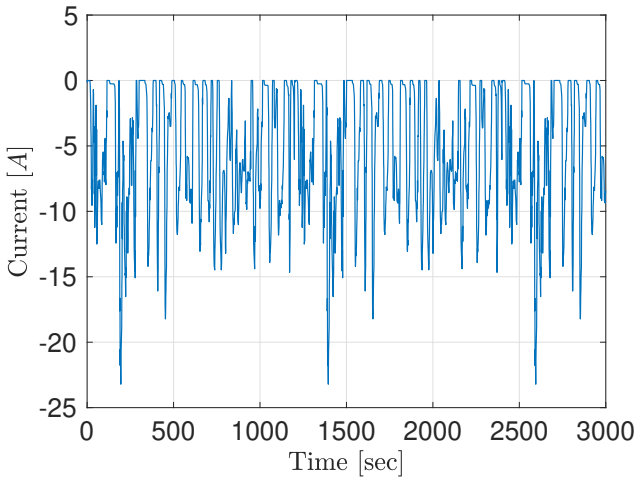

Fig. 5. Current input profile $I(t)$ applied to the ECM.

5. NUMERICAL RESULTS

This section presents the results obtained by applying the interval state estimation method to the considered Li-ion cell during the charging phase with an input profile as in Fig. 5.

The initial state set $[\bar{X}](0)$ is centered in the initial state condition $(z(0), V_{c1}(0)) = (0.3, 0)$. We consider an initial state uncertainty of 1% for the SOC and a much lower uncertainty on the voltage V_{c1} of $0.0001\% V$. This is justified by assuming that the battery is in stationary condition at $t = 0$ after a rest period (see Remark 1). The open loop state estimation is computed using only the prediction step (12) with natural inclusion function [4], at each time step k. Fig. 6 depicts a comparison between state sets computed in open loop (pink) and closed loop (green) respectively, highlighting the result obtained after the refinement procedure related to FBCP.

A further comparison between open and closed loop estimation is also shown in Fig. 7, in which the areas of the enclosures are calculated at each time k. Note that, despite the improved accuracy, the sets mildly increase over time. This is due to the increase of the SOC with time due to charging, which results in more conservative interval enclosure of the polynomial (16). As it can be noticed, the use of the FBCP approach (closed-loop) significantly reduces the size of the obtained intervals and still guarantees that the real state trajectory $\mathbf{x}(k)$ (depicted in blue in Fig. 6) belongs to $[\hat{X}(k)]$. The simulation has been done with Matlab 2020a, while all interval operations were performed using INTLAB 9 (Rump, 1999). The plots in Fig. 6 has been done using MPT (Kvasnica et al., 2004).

6. CONCLUSION

This paper developed a discrete-time interval observer for a single cell Li-ion battery based on Jaulin et al. (2001). Parameters have been identified by mean of least squares method using voltage data collected on an SPMe. Parametric uncertainties have been derived exploiting FIM, whose inverse approximates the covariance of the parameters. A variable transformation of the parameters have been performed to take their correlation into account. Results demonstrate tight enclosures on the states over time, which is corroborated by comparing open and closed loop state estimation. Future work will consider the ageing and temperature dynamics to address the degradation and safety of the cell, as well as the application of set-based estimation to battery packs, the usage of a different set representation to reduce the conservativeness, and perform joint state and parameter estimation.

[4] This is equivalent to replace each variable by its interval enclosure and apply elementary interval operations (Moore et al., 2009).

ACKNOWLEDGEMENTS

This work was supported by the italian National Agency for New Technologies, Energy and Sustainable Economic Development (ENEA) and Regione Lombardia. In particular, the assistance provided by Eng. Antonino Genovese was greatly appreciated.

REFERENCES

Alamo, T., Bravo, J.M., Redondo, M.J., and Camacho, E.F. (2008). A set-membership state estimation algorithm based on DC programming. *Automatica*, 44(1), 216–224.

Andersson, J.A.E., Gillis, J., Horn, G., Rawlings, J.B., and Diehl, M. (2019). CasADi – A software framework for nonlinear optimization and optimal control. *Mathematical Programming Computation*, 11(1), 1–36.

Bizeray, A.M., Zhao, S., Duncan, S.R., and Howey, D.A. (2015). Lithium-ion battery thermal-electrochemical model-based state estimation using orthogonal collocation and a modified extended Kalman filter. *Journal of Power Sources*, 296, 400–412.

Di Domenico, D., Stefanopoulou, A., and Fiengo, G. (2010). Lithium-ion battery state of charge and critical surface charge estimation using an electrochemical model-based extended kalman filter. *Journal of Dynamic Systems, Measurement, and Control*, 132(6).

Hansen, E. and Walster, G.W. (2003). *Global optimization using interval analysis: revised and expanded.* CRC Press.

Hu, X., Cao, D., and Egardt, B. (2018). Condition monitoring in advanced battery management systems: Moving horizon estimation using a reduced electrochemical model. *IEEE/ASME Transactions on Mechatronics*, 23(1), 167–178.

Jaulin, L., Braems, I., Kieffer, M., and Walter, E. (2001). Nonlinear state estimation using forward-backward propagation of intervals in an algorithm. In *Scientific Computing, Validated Numerics, Interval Methods*, 191–201. Springer.

Kim, I.S. (2009). A technique for estimating the state of health of lithium batteries through a dual-sliding-mode observer. *IEEE Transactions on Power Electronics*, 25(4), 1013–1022.

Kvasnica, M., Grieder, P., Baotić, M., and Morari, M. (2004). Multi-parametric toolbox (MPT). In *International Workshop on Hybrid Systems: Computation and Control*, 448–462. Springer.

Lu, L., Han, X., Li, J., Hua, J., and Ouyang, M. (2013). A review on the key issues for lithium-ion battery management in electric vehicles. *Journal of Power Sources*, 226, 272–288.

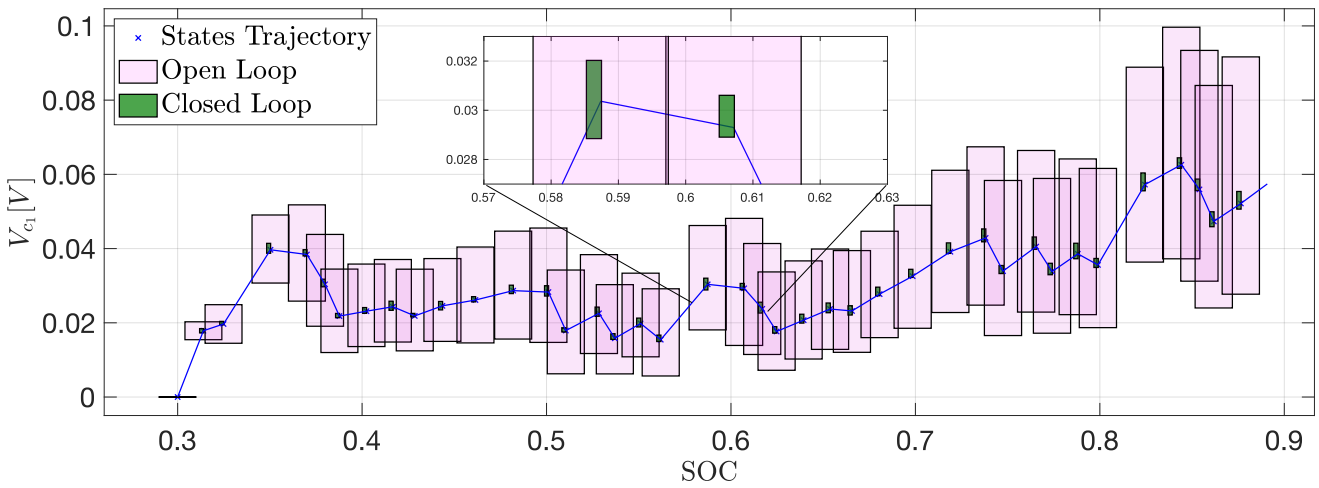

Fig. 6. Enclosures obtained using interval state estimation.

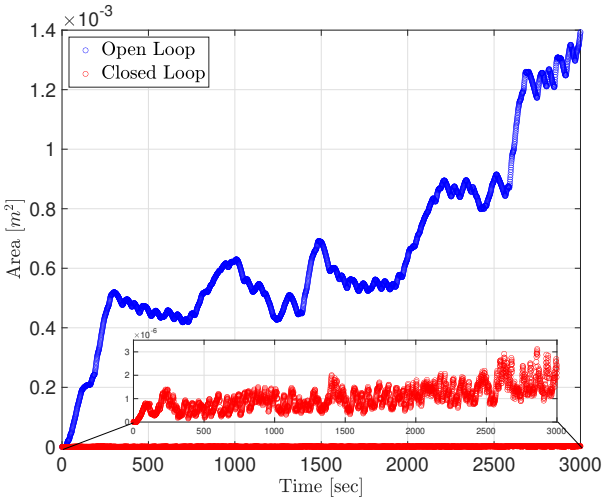

Fig. 7. Area of the estimated enclosures over time.

Moore, R.E., Kearfott, R.B., and Cloud, M.J. (2009). *Introduction to Interval Analysis*. SIAM, Philadelphia, PA, USA.

Perez, H.E., Hu, X., Dey, S., and Moura, S.J. (2017). Optimal charging of Li-ion batteries with coupled electro-thermal-aging dynamics. *IEEE Transactions on Vehicular Technology*, 66(9), 7761–7770.

Piller, S., Perrin, M., and Jossen, A. (2001). Methods for state-of-charge determination and their applications. *Journal of Power Sources*, 96(1), 113–120.

Plett, G.L. (2006). Sigma-point kalman filtering for battery management systems of lipb-based hev battery packs: Part 2: Simultaneous state and parameter estimation. *Journal of Power Sources*, 161(2), 1369–1384.

Pozzi, A., Ciaramella, G., Volkwein, S., and Raimondo, D.M. (2018). Optimal design of experiments for a lithium-ion cell: parameters identification of an isothermal single particle model with electrolyte dynamics. *Industrial & Engineering Chemistry Research*, 58(3), 1286–1299.

Rego, B.S., Raffo, G.V., Scott, J.K., and Raimondo, D.M. (2020). Guaranteed methods based on constrained zonotopes for set-valued state estimation of nonlinear discrete-time systems. *Automatica*, 111, 108614.

Rump, S.M. (1999). Intlab – INTerval LABoratory. In *Developments in reliable computing*, 77–104. Springer.

Shamma, J.S. and Tu, K.Y. (1997). Approximate set-valued observers for nonlinear systems. *IEEE Transactions on Automatic Control*, 42(5), 648–658.

Tulsyan, A., Tsai, Y., Gopaluni, R.B., and Braatz, R.D. (2016). State-of-charge estimation in lithium-ion batteries: A particle filter approach. *Journal of Power Sources*, 331, 208–223.

Weber, R.M., Spragg, R., Hoffmann, K., and Onori, S. (2019). Process noise quantification in kalman filters with application to electrochemical lithium-ion battery state estimation. In *Proc. of 2019 IEEE International Symposium on Industrial Electronics*, 1995–2000.

Xiong, R., Cao, J., Yu, Q., He, H., and Sun, F. (2017). Critical review on the battery state of charge estimation methods for electric vehicles. *Ieee Access*, 6, 1832–1843.

Zhang, D., Couto, L.D., Gill, P., Benjamin, S., Zeng, W., and Moura, S.J. (2020). Interval observer for SOC estimation in parallel-connected Lithium-ion batteries. In *2020 American Control Conference*, 1149–1154.